Cytokine 127 (2020) 154974

Contents lists available at ScienceDirect

Cytokine

journal homepage: www.elsevier.com/locate/cytokine

Multi-phase catheter-injectable hydrogel enables dual-stage protein-engineered cytokine release to mitigate adverse left ventricular remodeling following myocardial infarction in a small animal model and a large animal model

Amanda N. Steele[a,b], Michael J. Paulsen[b], Hanjay Wang[b], Lyndsay M. Stapleton[a,b], Haley J. Lucian[b], Anahita Eskandari[b], Camille E. Hironaka[b], Justin M. Farry[b], Samuel W. Baker[d], Akshara D. Thakore[b], Kevin J. Jaatinen[b], Yuko Tada[c], Michael J. Hollander[a], Kiah M. Williams[b], Alexis J. Seymour[a], Kailey P. Totherow[b], Anthony C. Yu[e], Jennifer R. Cochran[a], Eric A. Appel[e], Y. Joseph Woo[a,b,*]

[a] Department of Bioengineering, Stanford University, Stanford, CA 94305, United States
[b] Department of Cardiothoracic Surgery, Stanford University, Stanford, CA 94304, United States
[c] Department of Cardiovascular Medicine, Stanford University, Stanford, CA 94305, United States
[d] Department of Comparative Medicine, Stanford University, Stanford, CA 94304, United States
[e] Department of Materials Science & Engineering, Stanford University, Stanford, CA 94305, United States

ARTICLE INFO

Keywords:
Cytokines
Shear-thinning
Hydrogel
Minimally-invasive
Myocardial infarction
Angiogenesis

ABSTRACT

Although ischemic heart disease is the leading cause of death worldwide, mainstay treatments ultimately fail because they do not adequately address disease pathophysiology. Restoring the microvascular perfusion deficit remains a significant unmet need and may be addressed via delivery of pro-angiogenic cytokines. The therapeutic effect of cytokines can be enhanced by encapsulation within hydrogels, but current hydrogels do not offer sufficient clinical translatability due to unfavorable viscoelastic mechanical behavior which directly impacts the ability for minimally-invasive catheter delivery. In this report, we examine the therapeutic implications of dual-stage cytokine release from a novel, highly shear-thinning biocompatible catheter-deliverable hydrogel. We chose to encapsulate two protein-engineered cytokines, namely dimeric fragment of hepatocyte growth factor (HGFdf) and engineered stromal cell-derived factor 1α (ESA), which target distinct disease pathways. The controlled release of HGFdf and ESA from separate phases of the hyaluronic acid-based hydrogel allows extended and pronounced beneficial effects due to the precise timing of release. We evaluated the therapeutic efficacy of this treatment strategy in a small animal model of myocardial ischemia and observed a significant benefit in biological and functional parameters. Given the encouraging results from the small animal experiment, we translated this treatment to a large animal preclinical model and observed a reduction in scar size, indicating this strategy could serve as a potential adjunct therapy for the millions of people suffering from ischemic heart disease.

1. Introduction

Ischemic heart disease affects over 18.2 million Americans, and the prevalence is predicted to grow an additional 17% by 2030 [1]. Though gold standard treatments—including pharmacologic, revascularization, and surgical reconstructive strategies—have significantly improved overall mortality following myocardial infarction (MI), many patients will ultimately succumb to end-stage heart failure [2]. This is largely due to the fact that mainstay treatments do not adequately address the underlying pathophysiology and microvascular perfusion deficit that lead to maladaptive left ventricular remodeling and chronic heart failure after MI [3–5]. Post-MI patients who have robust coronary collateralization demonstrate improved regional function, highlighting the therapeutic role of angiogenesis [6–8]. Further, microvascular

* Corresponding author at: Department of Cardiothoracic Surgery, Falk Bldg, 870 Quarry Rd Ext, CV-235, Stanford, CA 93405, United States.
E-mail address: joswoo@stanford.edu (Y.J. Woo).

https://doi.org/10.1016/j.cyto.2019.154974
Received 1 November 2019; Received in revised form 18 December 2019; Accepted 26 December 2019

perfusion and performance predicts the functional recovery of ischemic tissue and subsequent clinical outcomes for the patient [9,10].

Angiogenic cytokine therapy has been investigated widely over the last few decades as a microrevascularization strategy that may work synergistically with current macrorevascularization techniques [11]. A number of angiogenic growth factors and cytokines have been evaluated with varying degrees of efficacy [11–16], yet, none have successfully been translated to the clinic. Limitations of direct cytokine infusion and injection include diffusion away from the intended region of interest and rapid degradation by proteases, effectively reducing the half-life and therapeutic effect. Further, because angiogenesis is a complex, multi-step process [17], delivery of multiple factors may be necessary to adequately restore the microcirculation and produce a clinically significant result [12].

An effective means of prolonging the delivery of cytokines, increasing their half-lives, protecting them from proteases, and localizing the delivery to the therapeutic region is to utilize a hydrogel. Hydrogels are water-swollen networks of insoluble polymers that can serve as *in vivo* drug-releasing depots, providing temporal and spatial control over release, while protecting the integrity of the cytokine [3,18–20]. However, a majority of hydrogels have limited ability for minimally-invasive delivery, require complex chemical functionalization or protein engineering, and cannot easily be scaled, hindering the clinical translatability [21–23]. Recently, we developed a novel, catheter-deliverable hydrogel which demonstrates impressive shear-thinning and self-healing behavior created from FDA-approved, biocompatible products [24]. This hydrogel is based on a hydrophobically-modified hyaluronic acid (HA) backbone that is cross-linked by poly(ethylene glycol)-*block*-poly(lactic acid) (PEG-PLA) core-shell nanoparticles, which can easily be scaled to clinical volumes due to the simple two-step chemical functionalization process. Further, due to the unique intrinsic multi-phase properties of this hydrogel, there is potential to load therapeutics with distinct drug release profiles, offering control over therapeutic timing.

Given the unique and unparalleled advantages of this clinically translatable hydrogel, we sought to evaluate the spatio-temporal delivery of two protein-engineered cytokines in a small animal model of myocardial infarction. The first factor is an engineered dimeric fragment of hepatocyte growth factor (HGFdf) that exhibits enhanced stability and expression yield compared to full-length recombinant hepatocyte growth factor (HGF) [25–28]. The therapeutic effects of HGF are well-documented, and include anti-apoptotic, anti-fibrotic, pro-angiogenic, and cardiomyogenic properties [11,15,23,26,27,29–31]. Additionally, stromal cell-derived factor 1α (SDF) is a potent chemoattractant for CD34+ stem cells, including endothelial progenitor cells (EPC), and exhibits marked pro-angiogenic and wound healing effects [13,31–37]. Therefore, the second cytokine under examination for dual-stage release from the hydrogel is an engineered analog of SDF (ESA) which has demonstrated improved stability and function, simpler synthesis, and lower production cost [8,36–38]. Following examination in a small animal model, we also sought to evaluate clinical translatability by investigating this dual-treatment in a large animal model, thereby better recapitulating the real-world application of this therapy.

In this report, we aim to overcome the current challenges associated with cytokine delivery which have prevented clinical translation. We hypothesized that dual-stage release of HGFdf and ESA would enable sustained, targeted delivery, activating separate but synergistic reparative pathways to yield an optimized therapeutic effect following myocardial infarction in both small and large animals. This treatment strategy significantly improves the translatability of therapeutic protein delivery to the heart by utilizing a catheter-deliverable hydrogel in combination with protein-engineered, optimized cytokines.

2. Materials & Methods

2.1. In vitro cytokine activity

To evaluate the activity of the combined cytokines, neonatal rat heart cells were isolated via the Pierce™ Primary Cardiomyocyte Isolation Kit (ThermoFisher) according to the manufacturer's instructions. Cardiac fibroblasts were removed by pre-plating the cells prior to plating the cardiomyocytes in a 96-well plate (CellTreat) at a density of 100,000 cells per well. After 24 h, the media was changed to serum-free DMEM and cells were treated with either 10 μM HGFdf (n = 12), 10 μM HGFdf + 25 μM ESA (n = 12), or were left untreated (n = 12). The cells were then placed in a hypoxic environment for 4 h at 1% oxygen, 5% carbon dioxide, 60% humidity and 37 °C (X3 Hypoxia Hood and Culture Combo from Xvivo System). After incubation, to assess apoptosis, Caspase-Glo® 3/7 Assay System reagent (Promega, G8091) was added to each well in equal parts as the media already present. The plate was placed in a normoxic incubator at 37 °C for 30 min. Following incubation, contents of the 96-well plate were mixed and transferred to a white 96-well plate to be read on a luminescent plate reader (Synergy 2 BioTek Microplate reader, BioTek Instruments) to quantify apoptosis.

Human bone marrow mononuclear cells were purchased from Lonza and plated on vitronectin-coated 10-cm plates and cultured in EGM™-2 Endothelial Growth Medium-2 (Lonza) in order to select for the EPC cell type [38,39]. Cells were grown to confluency over a time period of approximately three weeks. Once confluent, a cell migration assay (CytoSelect CBA-106) was used to test cell motility. EPCs were trypsinized, scraped, and applied to the membrane chamber while treatments were applied to the feeder tray: untreated (n = 12), 25 μM ESA (n = 12), or 10 μM HGFdf + 25 μM ESA (n = 12). The cells were placed in a hypoxic environment for 4 h at 1% oxygen, 5% carbon dioxide, 60% humidity, and 37 °C (X3 Hypoxia Hood and Culture Combo from Xvivo System). After incubation, cell detachment and lysis buffers were added according to the provided protocol. Solution was transferred to a black clear bottom 96-well plate and cell migration was quantified using a fluorescent plate reader (Synergy 2 BioTek Microplate reader, BioTek Instruments).

2.2. In vitro angiogenesis

To analyze *in vitro* angiogenesis, human umbilical vein endothelial cells (HUVECs) were resuspended in endothelial basal medium (Lonza) and plated on 24-well Matrigel® coated plates at 75,000 cells/well. Cells were then treated with 10 μM HGFdf (n = 6), 25 μM ESA (n = 6), or 10 μM HGFdf + 25 μM ESA (n = 6), or left untreated (n = 6). The cells were allowed to grow for 24 h, after which the cells were fixed with 4% paraformaldehyde, 1% glutaraldehyde solution, and then permeabilized with 0.25% Triton X-100. The cells were then stained with DAPI and rhodamine phalloidin. The extent of tubule and network formation was evaluated using a DMi8 Leica microscope by counting the number of junctions and branches, and by measuring network length [40].

2.3. Hydrogel synthesis and formation

Hyaluronic acid was converted to its tetrabutylammonium salt (HA-TBA) as published previously [24,41]. Briefly, 1 MDa sodium hyaluronate (NaHA) (Lifecore) was dissolved in deionized H_2O (diH_2O) to create a 1 w/v% solution. Upon complete dissolution, Dowex 50 W proton exchange resin (Acros Organics) was added to the solution (3 g resin per 1 g NaHA) and allowed to exchange for 6 h. The resin was removed by centrifugation and the solution was titrated to a pH ~ 9 with TBA-OH (Fisher Scientific O4575-100). The resulting solution was frozen at −80 °C, lyophilized, and stored long-term at −20 °C. To functionalize the HA, HA-TBA was dissolved in dimethyl sulfoxide at a concentration of 0.5 w/v%. The solution was heated homogenously to

45 °C and then dodecylamine ($-C_{12}$) and N,N′-diisopropylcarbodiimide were added in 1.3 molar excess to the HA-TBA repeat unit to create HA-C_{12}. The reaction proceeded for 24 h, at which point the solution was transferred to 3.5 kDa dialysis tubing and dialyzed against 0.0325 mM NaCl for 24 h. Finally, the solution was dialyzed against diH_2O for 3 days. The resulting solution was frozen at −80 °C, lyophilized, and stored long-term at −20 °C.

Biodegradable poly(ethylene glycol)-block-poly(lactic acid) (PEG–PLA) nanoparticles were created via an established protocol [24,42]. Briefly, 250 mg of 5 kDa PEG and 10 μL of 1,8-diazabicyclo [5.4.0]undec-7-ene (DBU) were dissolved in 1 mL dichloromethane (DCM). Lactide (1 g) was dissolved in 3 mL of DCM, and the resulting solution was added to PEG/DBU solution and stirred rapidly for 15 min. The reaction was quenched by adding the reaction solution to a solution of 15 mL of hexane and 15 mL of diethyl ether and subsequently vortexed. The hexane/ether solution was decanted, and the remaining PEG–PLA was dried overnight in a desiccator. To create nanoparticles (NPs), 50 mg dried PEG–PLA was dissolved in 1 mL DMSO and the solution was added dropwise to MilliQ water at a rapid stir rate. Resulting NPs were concentrated via filter ultracentrifugation (MWCO 10 kDa, Millipore Amicon Ultra-15) followed by resuspension in MilliQ water to a final concentration of 150 mg/mL.

Hydrogels were prepared by dissolving the HA-C_{12} polymer in MilliQ water to give a 6 wt% solution. The HA-C_{12} solution was then mixed with 15 wt% NP solution to give a final solution of 2 wt% HA-C_{12} and 10 wt% NPs. The final solution was mixed vigorously to ensure homogenous distribution and then vortexed to remove air bubbles.

2.4. Hydrogel encapsulation of cytokines

To encapsulate ESA within the NP phase of the hydrogel, 100 μg of ESA was dissolved into a solution of 50 mg PEG-PLA in 1 mL DMSO. The subsequent solution was then co-nanoprecipitated by dropwise addition into 10 mL MilliQ water as described previously [24]. Hydrogels were then prepared as described above by mixing a final solution of 2 wt% HA-C_{12} and 10 wt% NPs in the presence of HGFdf. Hydrogels were formed in 100 μL aliquots with a final amount of 25 μg ESA and 16 μg HGFdf per hydrogel [38,40].

2.5. Hydrogel mechanics

Rheological characterization was performed using a TA Instruments DHR-2 hybrid rheometer fitted with a Peltier stage. Oscillatory frequency sweep measurements were conducted between 0.1 and 100 rad s^{-1} with a torque of 2 μN·m. Flow rate sweep measurements were conducted with shear rates between 0.1 and 1000 s^{-1}. All tests were performed using a 20 mm plate geometry and a Peltier temperature of 37 °C with a gap height of 1000 μm. Analysis was performed using TA Instruments TRIOS software.

2.6. Hydrogel erosion

In vitro hydrogel erosion was assessed via uronic-acid based, colorimetric assay as published previously [20,24,43]. Briefly, 100 μL of hydrogel was added to a 1.5 mL Eppendorf tube and centrifuged to remove any entrapped air. Subsequently 1 mL of PBS was added to the tube (n = 4). At days 3, 7, 10, and 14, the PBS was removed and collected before being replaced with 1 mL of fresh PBS. The uronic acid concentration was measured using a carbazole reaction by adding 50 μL of each sample to a glass vial followed by 1 mL of ice-cold 25 mM sodium tetraborate in concentrated sulfuric acid. Vials were then incubated for 10 min at 100 °C and then cooled on ice, at which point, 30 μL of 0.125 (w/v)% carbazol (Sigma-Aldrich,C5132) in absolute ethanol was added before briefly vortexing. Vials were then incubated for 15 min at 100 °C and then allowed to cool to room temperature. Finally, 200 μL of the solution was transferred to a 96-well plate for measurement. The absorbance at 525 nm was read using a plate reader (Synergy 2 BioTek Microplate reader, BioTek Instruments).

2.7. Custom cytokine synthesis

HGFdf was synthesized and characterized as previously reported [28,40]. Briefly, the DNA encoding HGFdf was cloned into the pPIC9K plasmid (Life Technologies, Grand Island, NY) and transformed into the Pichia pastoris vector strain GS115. Colonies that survived geneticin selection were inoculated and induced with methanol for 3 days. Yeast cells were pelleted by centrifugation, and the supernatant collected for Ni-nitrilotriacetic acid affinity chromatography. The elution fractions containing HGFdf were buffer-exchanged into 1 × PBS + 500 mM NaCl (PBS500) and further purified with size exclusion chromatography using a Superdex 75 10/300 GL (GE Healthcare, Pittsburgh, PA). Protein purity was analyzed using 12% Tris-Glycine SDS-PAGE (Life Technologies, Grand Island, NY). Protein was flash-frozen in 0.01% Tween80 in PBS500 and stored at −80 °C. Thawed protein was kept at 4 °C and used within 3 weeks.

ESA is a minimized, highly-efficient engineered version of SDF and contains the CXCR4 receptor-binding N-terminus and the stabilizing C terminus linked via two proline residues [8,36–38]. This polypeptide is synthesized using solid-phase peptide synthesis, where the N α-amino acids are assimilated in a stepwise fashion (Anaspec, San Jose, CA).

2.8. In vitro cytokine release kinetics

To measure *in vitro* release kinetics of the encapsulated cytokines, both were fluorescently labeled. ESA was labeled with a Cyanine7 (Cy7) fluorescent tag during the synthesis process (Anaspec). HGFdf was labeled via the Alexa Fluor® 488 Microscale Protein Labeling Kit (A30006) according to the manufacturer's instructions. Briefly, 100 μg of HGFdf was titrated to a pH of ~8.3 with 1 M sodium bicarbonate. The Alexa Fluor® 488 TFP ester was added at a molar ratio of 60. The reaction was incubated for 15 min at room temperature. The labeled HGFdf was then separated from unreacted dye using spin filters and stored at 4 °C. The labeled cytokines were encapsulated into the hydrogel using the same procedure as described above.

To measure release, 100 μL hydrogels were formed (n = 4/group) and placed into 1.5 mL Eppendorf tubes and spun to remove air bubbles. Immediately following, 1 mL of PBS was placed on top of the hydrogel, and then sampled approximately daily. At the end of the assay time period, any remaining hydrogel was disrupted and sampled. Samples were stored at −20 °C until the end of the time period, at which point, all samples were thawed, vortexed and 100 μL of the sample was placed into a black 96-well plate. The samples were read at the appropriate wavelength (HGFdf: ex/em 485/528 nm, ESA: ex/em 750/773 nm) to determine release.

2.9. In vitro cytokine release activity

To determine the activity of the cytokines following release from the hydrogel, we examined the effect of the released cytokines on cardiomyocyte apoptosis and EPC migration. Cardiomyocytes were isolated from neonatal rat hearts as described above and plated in a 96-well plate at a density of 100,000 cells per well. Two days prior to cell treatment, 100 μL HA-NP gel and 100 μL HA-NP gel containing HGFdf and ESA were added into 0.4 μm pore transwells (CorningTranswell) and allowed to elute into 1 mL of serum-free DMEM (n = 6/group). At the start of the experiment 100 μL of eluant was transferred to the 24-well plate (n = 12/group) or 100 μL of untreated serum-free DMEM. The plate was placed in a hypoxic environment for 4 h at 1% oxygen, 5% carbon dioxide, 60% humidity, and 37 °C (X3 Hypoxia Hood and Culture Combo from Xvivo System). Following incubation, Caspase-Glo® 3/7 Assay System reagent (Promega, G8091) was added to each well in equal parts as the media already present. The cells were then

placed in an incubator at 37°C for 30 min according to the assay instructions. After 30 min, contents of the 24-well plate were transferred to a white 96-well plate to be read on a luminescent plate reader (Synergy 2 BioTek Microplate reader, BioTek Instruments).

Human bone marrow mononuclear cells were cultured as described previously to select for the EPC phenotype. Upon confluency, EPCs were lifted with trypsin, scraped off the plate, and added to the membrane chamber of the assay while the above treatments (serum free DMEM, HA-NP eluant, or HA-NP containing cytokines eluant) were applied to the feeder tray. The cells were placed in a hypoxic environment for 4 h at 1% oxygen, 5% carbon dioxide, 60% humidity, and 37 °C (X3 Hypoxia Hood and Culture Combo from Xvivo System). Following incubation, cell detachment and lysis buffers were added according to the assay protocol. Solution was transferred to a black clear bottom 96-well plate and cell migration was quantified using a fluorescent plate reader (Synergy 2 BioTek Microplate reader, BioTek Instruments).

2.10. Small animal model of myocardial infarction

All animal experiments were conducted in accordance with the Guide for the Care and Use of Laboratory Animals, published by the US National Institute of Health. The protocol was approved by the Administrative Panel on Laboratory Animal Care of Stanford University (protocol #28921). Adult male Wistar rats weighing 250–300 g were obtained from Charles River Laboratories (Wilmington, MA). Rats were sedated via 2% isoflurane, endotracheally intubated with a 16-gauge angiocatheter and mechanically ventilated with 1.5% isoflurane. The heart was exposed via left thoracotomy and an MI was induced via permanent ligation of the left anterior descending artery 1–2 mm below the left atrial appendage. Immediately following ligation, animals received 100 μL injection of PBS (n = 14), 16 μg HGFdf + 25 μg ESA in 100 μL PBS (HGFdf + ESA only) (n = 13), 100 μL of HA-NP hydrogel alone (HG only) (n = 13), or 100 μL of HA-NP hydrogel containing 16 μg HGFdf + 25 μg ESA (HG + HGFdf + ESA) (n = 15). The thoracotomy was closed with 4–0 polypropylene suture, sustained release buprenorphine (0.5 mg/kg) was given for analgesia, and animals were recovered.

2.11. Left ventricular echocardiographic functional assessment

Left ventricular (LV) function was evaluated at 4 weeks using a VisualSonics Vevo 2100 (FUJIFILM Visual Sonics Inc, Ontario, Canada) digital imaging system with a MS250 transducer (13 MHz). LV parasternal short-axis B-mode and M-mode images were acquired at two levels within the LV (mid-papillary and between the papillary muscles and apex). Image acquisition and all analyses were performed by a single, blinded investigator.

2.12. Histological analysis and immunohistochemistry

Following functional assessment, animals underwent a terminal procedure. Rats were sedated via 2% isoflurane on nose cone. Hearts were exposed via a median sternotomy and arrested with KCl. The hearts were explanted, flushed with PBS, and filled retrograde with Tissue Tek optimum cutting temperature (OCT) compound (Sekura, The Netherlands), frozen, and stored at −80 °C. Twenty 10-μm-thick sections were prepared from each heart at four different levels throughout the infarct.

To determine infarct size, two sections at the level of the mid-papillary were stained with Masson's trichrome (n = 12/group). Standard digital photographs were taken with an Epson V550 Color Scanner (Epson, Long Beach, CA). Photographs were uploaded to ImageJ, and the size of the infarct was calculated as the percent of total circumference and total area of the LV. To examine vessel density in the infarct borderzone, three 10-μm-thick sections were stained with antibodies directed against α-smooth muscle actinin (SMA) (1:200), VE-cadherin (VECAD) (1:200), and troponin (1:200) (Abcam) to quantify vessel density in the infarct and borderzone (n = 10/group). Heart sections were fixed with 4% paraformaldehyde, blocked with 10% fetal bovine serum, incubated with primary antibodies, and then stained with fluorescent secondary antibodies (1:200) (Alexa Fluor 488, Alex Fluor 594, and Alex Fluor 647). A Zeiss confocal microscope and a 10× objective was used to obtain images of the entire heart section. Mature arterioles were defined by: (1) a visible lumen, (2) lumen diameter of 10–100 μm, and (3) positive α-SMA staining.

2.13. In situ release

In a subset of animals, *in situ* fluorescence of HA-NP, ESA, and HGFdf was qualitatively measured using a Pearl Triology small animal imaging system, model #9430 (LI-COR, Lincoln, NE). ESA was labeled with a Cyanine7 (Cy7) fluorescent tag during the synthesis process (Anaspec). HGFdf was labeled via the Alexa Fluor® 488 Microscale Protein Labeling Kit (A30006) according to the manufacturer's instructions and as described above, with the exception of utilizing an Alexa Fluor™ 790 NHS Ester instead of the Alexa Fuor® 488 TFP ester included within the kit. Finally, the HA backbone of the HA-NP hydrogel was fluorescently labeled using a functionalization reaction based on a previously published protocol [44]. 1 MDa HA-C_{12} was dissolved 0.5 wt% in diH_2O and the pH was titrated to 10 using 1 M NaOH. A 5-fold molar excess of ethylene sulfide was added dropwise and stirred vigorously for 18 h. The resulting solution was filtered through a bed of Celite® 545 and a 5-fold molar excess of DTT was added. The pH was titrated to 8.5 with 1 M NaOH and left to stir vigorously. After 24 h the pH was reduced to 3.5 with 6 N HCl. The solution was dialyzed against dilute HCl for 24 h (pH 3.5). The resulting solution was lyophilized for 4 days. The HA-C_{12}-SH solution was dissolved 0.5 wt% in TEA buffer with 5 mM TCEP, and once dissolved, dylight-800 maleimide (ThermoFisher cat#: 46621) was added and the solution was stirred for 2 h at 4 °C. After 2 h the solution was dialyzed against PBS overnight at 4 °C. The solution was then frozen at −80 °C and lyophilized.

Hydrogels were prepared as above by encapsulating the tagged ESA into the NP phase or mixing tagged HGFdf into the aqueous phase. Tagged HA-C_{12} polymer was mixed into 6 wt% aqueous solution and added normally to the NPs as described above. In order to measure each component, only one fluorescently labeled component was added into the hydrogel at a time. To examine *in situ* release, animals underwent the MI procedure as described above. Immediately following ligation, animals received 100 μL injections of either tagged HA-NP, HA-NP containing tagged ESA, or HA-NP containing tagged HGFdf (n = 2 per timepoint per group). Animals were recovered as mentioned. At defined timepoints following the surgery (day 1, 5, 7, 14, or 28), hearts were explanted and immediately read on the Pearl imaging system on the 800 nm channel.

2.14. Large animal model of myocardial infarction

Myocardial infarction was induced in 20 male Dorset sheep using an established and reproducible model [45]. Animals were sedated with intravenous diazepam (0.05–0.2 mg/kg) and anesthesia was maintained on inhaled isoflurane (1.5%-3%). Induction was completed with 5–12 mg/kg of propofol, at which point, animals were endotracheally intubated. Sustained release buprenorphine was given under sedation prior to the surgery, with one dose lasting 72 h for pain control. Animals underwent a pre-operative cardiac MRI to assess global ventricular function and geometry. General anesthesia was maintained for the entirety of the imaging procedure. Immediately following imaging, animals were returned to the operating suite and an anterior, mini thoracotomy was performed to access and expose the heart. A consistently-sized myocardial infarction was produced by ligating the distal

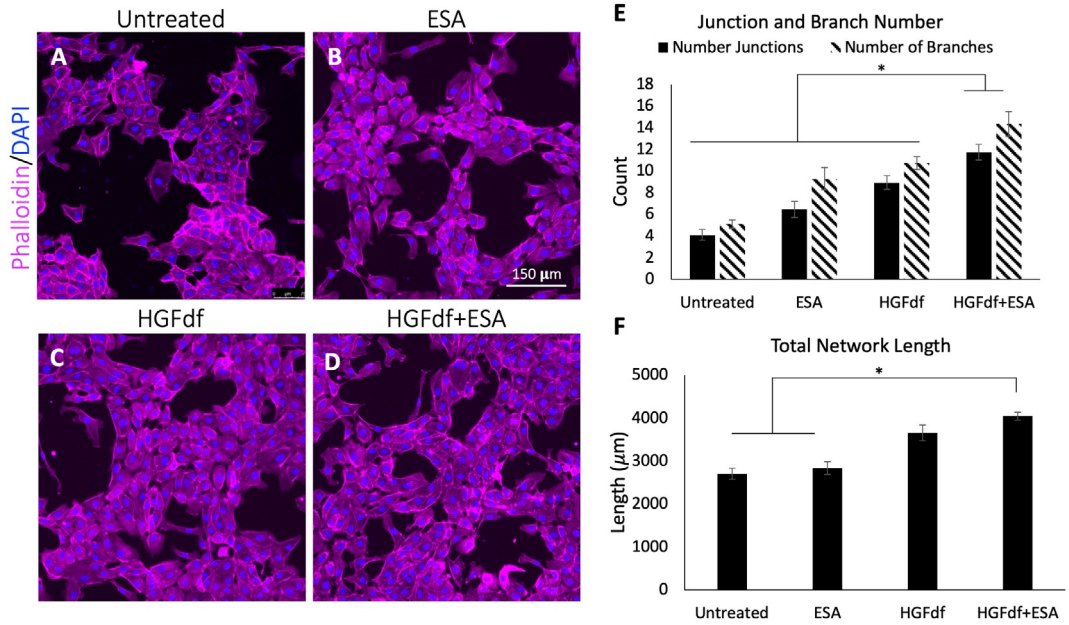

Fig. 1. Assessment of *in vitro* angiogenesis. Human umbilical cord vein endothelial cells were treated with (A) untreated, (B) engineered stromal cell-derived factor 1α (ESA), (C) engineered dimeric fragment of hepatocyte growth factor (HGFdf) or (D) a combination of HGFdf and ESA. The extent of network formation (E, F) was evaluated in all groups. Pairwise Student T-test with Bonferroni's correction, *$p < 0.05$.

left anterior descending coronary artery or its diagonal branches with a 5–0 polypropylene suture. At this stage, animals were randomized to receive a 1 mL injection of PBS (n = 6), 1 mL of HA-NP hydrogel alone (HG only) (n = 7), or 1 mL HA-NP hydrogel containing 300 µg of ESA and 1 mg of HGFdf (HGFdf + ESA) (n = 7). Treatments were injected into the epicardium through a custom 4-Fr angiocatheter secured with a 28-G insulin syringe needle. The doses of ESA and HGFdf administered were determined based on previously published studies [36,38,40]. Throughout the procedure, continuous ECG, oxygen saturation, respiratory rate, and core body temperature were measured. Animals were recovered from aesthesia and monitored for 8 weeks until the terminal procedure. After the 8-week timepoint, the animals were sedated and intubated as described above and underwent a final cardiac MRI to evaluate function and geometry. Following MRI and data acquisition, KCl (1 meq/kg) was administered for euthanasia. The heart was then explanted, imaged, and prepared for histological analysis.

2.15. Image acquisition and processing

MRI acquisition and analysis were performed by a single, blinded investigator. Cardiac MRI was performed using Signa HDx 3.0 T MRI scanner (GE Healthcare) and an 8-channel chest coil. The cine and late gadolinium enhancement (LGE) were acquired under ECG gating and breath-holding. Cine images were obtained with FIESTA sequence (TR 3.4 ms; TE min-full; flip angle 45°; thickness 8 mm; matrix 224 × 224; and field of view 35 cm). After Gd-DTPA (0.2 mmol/kg of Magnevist; Bayer Health Care Pharma AG, Berlin, Germany) was administered, LGE was obtained with fast gradient echo-inversion recovery (FGRE-IR) sequence (TR 6.2 ms; TE 2.9 ms; flip angle 15°; thickness 8 mm; matrix 224 × 192; field of view 35 cm; TI 250–300 ms) 10–25 min later.

MRI was analyzed on Medis Suite 3.0 (NC, USA). Endocardial and epicardial contours were traced semi-automatically to quantify LV end-diastolic volume (LVEDV), LV end-systolic volume (LVESV), LVEF, stroke volume (SV), cardiac output (CO), and LV muscular volume. LGE was quantified by standard deviation (SD) measurement (QMass 8.1). In this method, signals apart from 5SDs from the healthy remote areas was determined as LGE and quantified.

2.16. Statistical analysis

All variables are reported as mean ± standard deviation. In vitro data is analyzed via pairwise Student *t*-tests with a Bonferroni correction for multiple comparisons. *In vivo* data which approximated a normal distribution was analyzed via one-way ANOVA with a Bonferroni correction for multiple comparisons. Data that did not have equal variances were analyzed via one-way ANOVA with a Dunnet's T3 correction for multiple comparisons. Statistical significance was set at $p < 0.05$. Analyses were performed with IBM SPSS Statistics software package, version 25.0.

3. Results

3.1. Co-delivery of protein-engineered cytokines does not inhibit function

To determine that co-delivery of protein-engineered cytokines is a viable treatment strategy, we first sought to confirm that the two therapeutic pathways would not have an inhibitory effect on the other. To confirm that the addition of ESA to HGFdf would not affect HGFdf's anti-apoptotic function, we evaluated cardiomyocyte apoptosis (Supplementary Fig. 1A). There was no statistical difference in the reduction of apoptosis in cells treated with HGFdf (22% reduction) compared to HGFdf + ESA (25% reduction), but both treatments resulted in significantly decreased apoptosis compared to the untreated group. Next, we evaluated EPC migration in the presence of ESA or HGFdf + ESA (Supplementary Fig. 1B). The addition of HGFdf to ESA treatment did not affect the ability of ESA to induce migration in EPCs. Compared to the untreated group, ESA treatment and HGFdf + ESA resulted in a 17% and 19% respective increase in cellular migration compared to the untreated group.

3.2. Co-delivery of HGFdf and ESA results in significant tubule network formation

Due to the pro-angiogenic behavior of HGFdf and ESA, we evaluated the co-delivery of these cytokines to induce tubule formation *in vitro*. Human umbilical cord vein endothelial cells were treated with PBS, ESA, HGFdf, or HGFdf + ESA and various parameters were used to

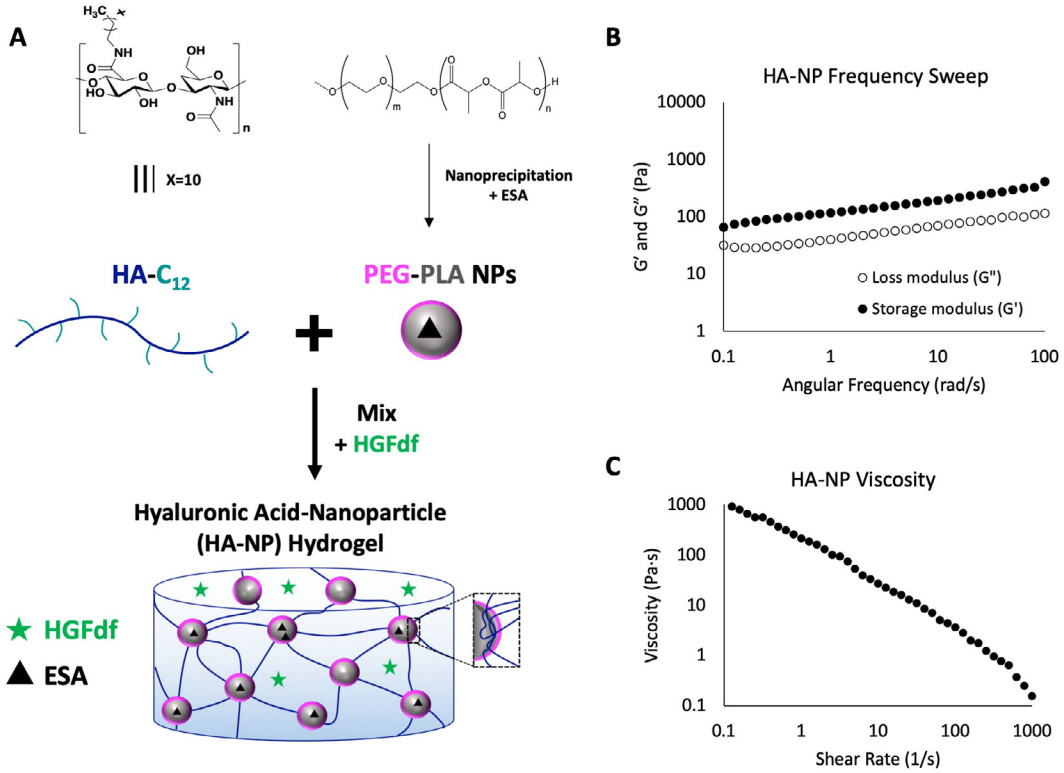

Fig. 2. Formation and mechanical behavior of the HA-NP hydrogel. (A) Demonstration of hydrogel formation with encapsulated cytokines. HA-NP hydrogel is composed of a hydrophobically-modified hyaluronic acid which is crosslinked by hydrophobic nanoparticles. The ESA is encapsulated into the nanoparticle phase and HGFdf is encapsulated into the aqueous phase of the hydrogel. (B) An oscillatory frequency sweep reveals the consistent solid-like behavior of the hydrogel. (C) The HA-NP hydrogel has an impressive and pronounced shear-thinning behavior indicated by the shear sweep.

assess network formation (Fig. 1). Co-delivery of HGFdf + ESA resulted in the most pronounced network formation due to significant increases in the number of junctions, number of branches, and total network length. Compared to the untreated group, there was a ~3-fold increase in the number of junctions and number of branches, and a 1.5-fold increase in the total network length. Co-delivery of HGFdf + ESA also induced significant increases in the number of junctions and branches (11.7 ± 2.4 junctions and 14.4 ± 3.8 branches) compared to both HGFdf (8.9 ± 2.1 junctions and 10.7 ± 2.0 branches, $p < 0.05$) and ESA alone (6.5 ± 2.5 junctions and 9.3 ± 3.4 branches, $p < 0.05$).

3.3. Gel formation and mechanics

The HA-NP hydrogel formed rapidly upon mixing aqueous solutions of the HA-C_{12} polymer and the PEG-PLA NPs (Fig. 2). Rheological characterization was performed to determine the hydrogel strength (Fig. 2B) and shear-thinning behavior (Fig. 2C). A frequency sweep revealed that tan δ, the ratio of loss modulus (G″) divided by the storage modulus (G′), was < 1 at all frequencies measured, indicating that the sample behaves as an elastic solid. The storage modulus at 10 rad/s was used to determine hydrogel strength. The hydrogel demonstrated a strength of 195 Pa. To examine the shear-thinning behavior, a shear-rate sweep revealed a uniform and pronounced decrease in viscosity from low to high shear rates. Finally, an erosion assay (Supplementary Fig. 2) determined the rate of release of the hydrogel backbone, with 47% of the hydrogel being eroded *in vitro* after 14 days.

3.4. In vitro release kinetics and activities of dual-cytokine delivery

The activity of both encapsulated cytokines was evaluated on relevant cell types (Fig. 3). Cardiomyocytes that were serum starved in hypoxia demonstrated a 30% decrease in apoptosis when treated with the HGFdf and ESA that were released by the HA-NP hydrogel compared to the untreated and HG only groups. Similarly, EPCs cultured in hypoxia exhibited a 112% increase in migration when treated with the cytokines released from the hydrogel compared to the untreated group. Due to the chemotactic properties of HA, the HA-NP hydrogel also induced a mild degree of migration (30% increase) relative to the PBS group.

In vitro release kinetics were measured for 28 days and 33 days for HGFdf and ESA release, respectively (Fig. 3C). At day 28, approximately 97% of the HGFdf had been released from the hydrogel, whereas on day 33, 52% of the ESA had been released. The two distinct profiles highlight the control over drug delivery via the method of encapsulation within the hydrogel.

3.5. HG + HGFdf + ESA significantly enhances border zone vessel density and reduces infarct size

Masson's trichrome analysis revealed that rats treated with the HG + HGFdf + ESA treatment exhibited a significantly reduced infarct size compared to the other groups (Fig. 4). The HG + HGFdf + ESA treated animals had an average infarct size of 28.9% ± 8.8% of the total LV circumference and 18.8% ± 5.5% of the total LV area ($p < 0.001$ compared to PBS). Conversely, animals given the PBS treatment had an average infarct size of 51.4% ± 13.1% of the total circumference and 39.6% ± 13.5% of the total area. Animals treated with HG only or HGFdf + ESA only also demonstrated infarct mitigation in both circumference and area compared to the PBS animals (HG only: 39.3% ± 4.7% and 27.1 ± 5.7%; HGFdf + ESA only: 41.8% ± 12.2% and 31.35 ± 9.5%, respectively).

In addition to improvement in infarct size, rats which received the HG + HGFdf + ESA treatment also demonstrated a significant increase in arteriole density within the border zone region (Fig. 5). The PBS

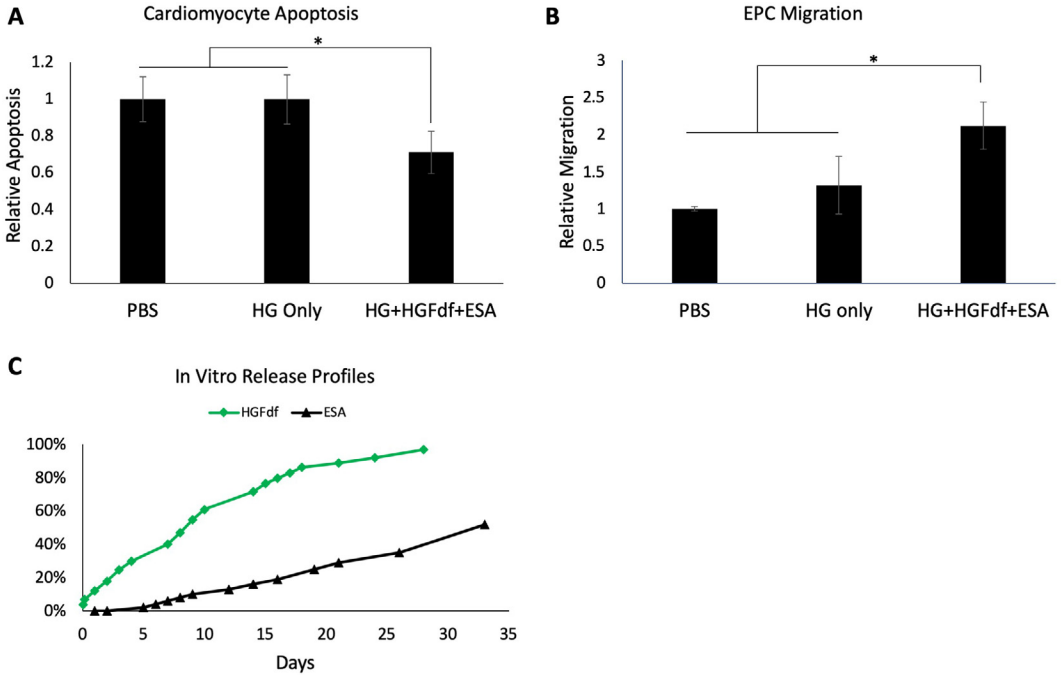

Fig. 3. Cytokine activity and release from the HA-NP hydrogel. (A) The bio-functionality of HGFdf after release from the HA-NP hydrogel was evaluated on cardiomyocytes that were serum-starved in hypoxia. Treatment with the HGFdf + ESA that had been released from the hydrogel resulted in a significant decrease in apoptosis. (B) HGFdf + ESA released from the hydrogel resulted in a significant increase in EPC migration. (C) The distinct release profiles of both the HGFdf and ESA from different phases from the HA-NP hydrogel over a period of a month. Pairwise Student T-test with Bonferroni's correction, *$p < 0.05$.

control animals exhibited an average of 3.0 ± 1.2 arterioles/mm^2 positively stained arterioles in the border zone whereas HG only animals and HGFdf + ESA only animals had a significant increase with 5.7 ± 1.6 arterioles/mm^2 and 5.8 ± 0.7 arterioles/mm^2, respectively. Finally, animals treated with HG + HGFdf + ESA had the most pronounced increase compared to the PBS group with 8.5 ± 1.6 arterioles/mm^2 arterioles.

3.6. HG + HGFdf + ESA mitigates left ventricular dilation and improves function

Echocardiographic investigation highlighted the geometric (Table 1) and functional (Table 2) improvements of the treatment groups. Four weeks following the procedure, rats which had been treated with HG + HGFdf + ESA demonstrated a preservation of left ventricular dimensions. The left ventricular inner diameter at end-systole of HG + HGFdf + ESA animals (5.87 ± 0.80 mm) was significantly improved compared to all other treatment groups: PBS, 7.45 ± 1.05 ($p < 0.001$); HG only 6.75 ± 0.61 ($p < 0.039$); HGFdf + ESA only 6.92 ± 0.79 ($p < 0.009$). Similarly, the left ventricular systolic area of the HG + HGFdf + ESA animals (31.75 ± 6.67 mm^2) was significantly reduced compared to the PBS (57.97 ± 21.04 mm^2, $p < 0.001$) and HG only (49.05 ± 8.5 mm^2; $p = 0.003$) groups. Finally, there was also an improvement in end-diastolic area. Animals treated with HG + HGFdf + ESA had an average diastolic area of 54.76 ± 6.61 mm^2, which was significantly improved compared to PBS animals (75.76 ± 20.52, $p < 0.001$) and HG only animals (71.04 ± 10.19, $p = 0.007$).

In addition to geometric parameters, there were also significant improvements in left ventricular function (Table 2). Animals treated

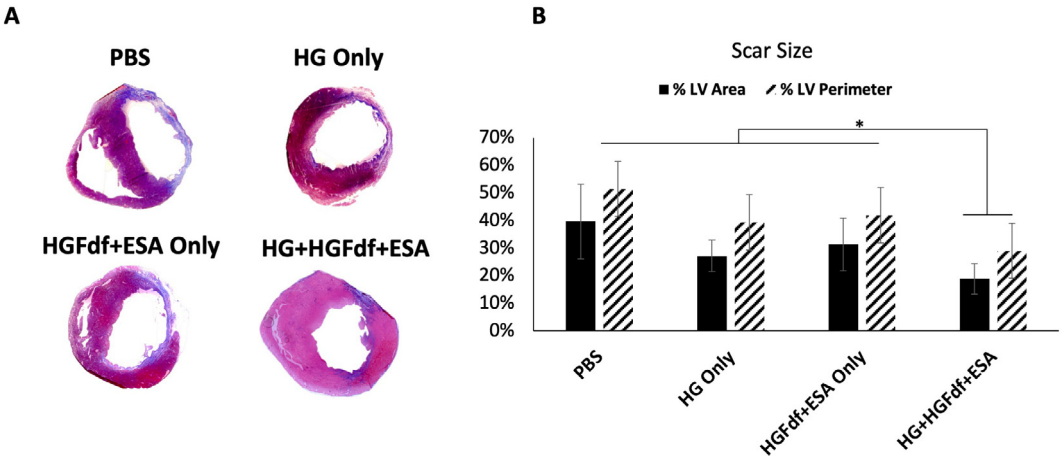

Fig. 4. Quantification of infarct size via Masson's Trichrome staining. (A) Representative sections from each treatment group. (B) Infarct size was calculated by transmural infarct of the entire left ventricular area (%LV area) and total circumference of the left ventricle (%LV Perimeter), ANOVA with a Bonferroni correction for multiple comparisons, *$p < 0.05$.

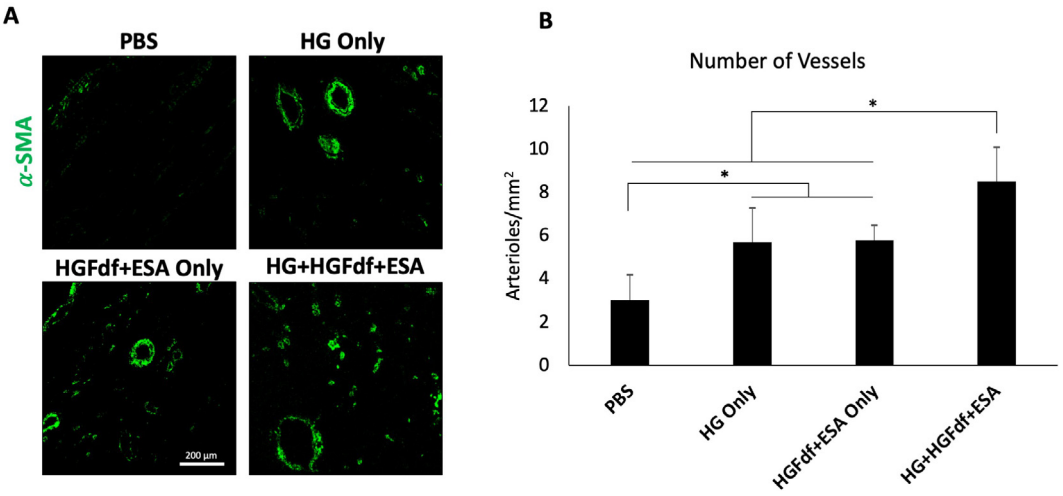

Fig. 5. Histological characterization and quantification of arteriole vessel density by positive α-smooth muscle actin (α-SMA) staining. (A) Representative confocal images of treatment groups in the border zone region. (B) Analysis of arteriole density revealed significant increase in HG + HGFdf + ESA group. ANOVA with a Bonferroni correction for multiple comparisons, *$p < 0.05$.

with HG + HGFdf + ESA demonstrated statistically significant improvements in all functional parameters measured compared to the other groups. At 4 weeks post-MI, HG + HGFdf + ESA animals had an average ejection fraction of 51.83 ± 6.96% compared to PBS (32.98 ± 6.92%, $p < 0.001$), HG only (42.80 ± 7.10%, $p = 0.012$), and HGFdf + ESA only (41.21 ± 8.67%, $p = 0.002$). There were also pronounced improvements in fractional shortening (28.00 ± 4.57%) and fractional area change (41.67 ± 8.18%) in the HG + HGFdf + ESA treatment group compared to all other treatments.

3.7. Qualitative in situ release

Using near-infrared wavelength fluorophores, we were able to obtain a signal from the tagged HA-NP hydrogel, tagged HGFdf encapsulated in the aqueous phase of the hydrogel, and tagged ESA encapsulated into the nanoparticle phase of the hydrogel (Supplementary Fig. 3). Because of the different chemical functionalization reactions required to tag each of the components, we cannot accurately compare between groups quantitatively. Nonetheless, it is important to note that the animals treated with the fluorescently tagged components maintained a strong fluorescent signal until day 14. At day 28, the signal had significantly decreased, but was still present within the heart tissue. These data confirm that we achieved a prolonged release of the encapsulated therapeutics.

4. Large animal scar size, function, and geometry

Given the promising results from the small animal study, the next goal was to determine the feasibility of clinical translation of this treatment strategy. Therefore, we scaled up production and validated this therapy in a large animal model. We treated male Dorset sheep with PBS, HG only, or HG + HGFdf + ESA immediately after induction of MI via a catheter-based, epicardial injection (Supplementary Fig. 4). Eight weeks following MI, we imaged the endocardial surface of the heart to determine transmural infarct size (Fig. 6). Sheep that had been treated with PBS had an average infarct size of 31.4 ± 6.1% which was significantly larger compared to HG + HGFdf + ESA treated sheep which demonstrated an infarct size of 15.9 ± 2.1% ($p < 0.01$). HG only sheep also had a decrease in scar size compared to the PBS treated sheep with an average size of 20.3 ± 3.5% of the total endocardial surface.

In addition to scar size, there were trends in improvement in left

Table 2
Left ventricular function four weeks post-MI.

	Fractional Area Change (%)	Ejection Fraction (%)	Fractional Shortening (%)
PBS	24.06 ± 7.37 $p < 0.001$	32.98 ± 6.92 $p < 0.001$	16.66 ± 3.73 $p < 0.001$
HG Only	30.39 ± 6.54 $p = 0.001$	42.80 ± 7.10 $p = 0.012$	22.33 ± 4.24 $p = 0.008$
HGFdf + ESA Only	33.58 ± 6.75p $= 0.025$	41.21 ± 8.67 $p = 0.002$	21.53 ± 5.18 $p = 0.002$
HG + HGFdf + ESA	41.67 ± 8.18	51.83 ± 6.96	28.00 ± 4.57

P values refer to comparison between HG + HGFdf + ESA group and the control groups: PBS, HG only, HGFdf + ESA only. Values are reported as mean ± standard deviation. ESA, engineered stromal-cell derived factor 1α; HG, hydrogel; HGFdf, hepatocyte growth factor dimeric fragment.

Table 1
Left ventricular geometry four weeks post-MI.

	LV Systolic Area (mm^2)	LV Diastolic Area (mm^2)	LVIDs (mm)	LVIDd (mm)	LV Volume Systole (mL)	LV Volume Diastole (mL)
PBS	57.97 ± 21.04 $p < 0.001$	75.76 ± 20.52 $p < 0.001$	7.45 ± 1.05 $p < 0.001$	8.92 ± 0.87 $p = 0.04$	302 ± 107.94 $p < 0.001$	445.89 ± 100.5 $p = 0.076$
HG Only	49.05 ± 8.5 $p = 0.003$	71.04 ± 10.19 $p = 0.007$	6.75 ± 0.61 $p < 0.039$	8.69 ± 0.55 $p = 0.263$	239.61 ± 51.22 $p = 0.129$	419.49 ± 58.64 $p = 0.401$
HGFdf + ESA Only	43.26 ± 7.73 $p = 0.084$	65.16 ± 7.64 $p = 0.140$	6.92 ± 0.79 $p < 0.009$	8.82 ± 0.58 $p = 0.107$	253.91 ± 72.19 $p = 0.041$	417.36 ± 89.36 $p = 0.401$
HG + HGFdf + ESA	31.75 ± 6.67	54.76 ± 6.61	5.87 ± 0.80	8.19 ± 0.78	176.42 ± 53.08	370.61 ± 72.42

P values refer to comparison between HG + HGFdf + ESA group and the control groups: PBS, HG only, HGFdf + ESA only. Values are reported as mean ± standard deviation. ESA, engineered stromal-cell derived factor 1α; HG, hydrogel; HGFdf, hepatocyte growth factor dimeric fragment; LVIDd, left ventricular inner diameter diastole; LVIDs, left ventricular inner diameter systole.

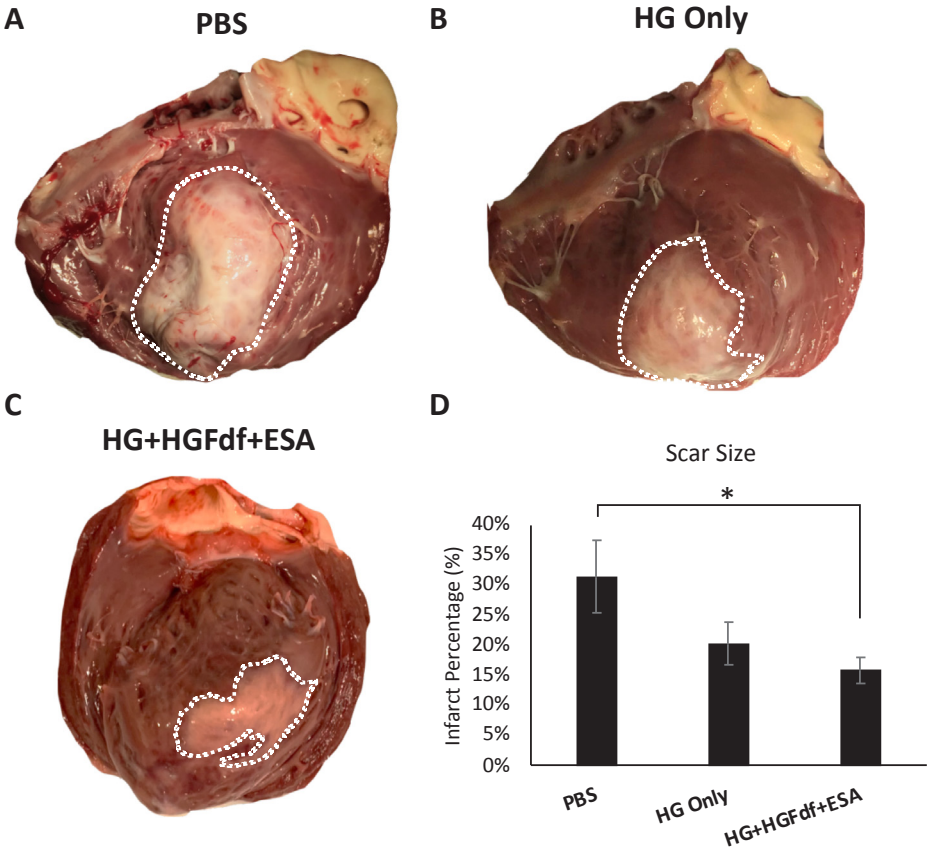

Fig. 6. Left ventricle infarct area. Hearts were explanted and opened longitudinally. The infarct was photographed for quantification and representative images of hearts from each group are presented. (A) PBS treated (B) HG only treated and (C) HG + HGFdf + ESA treated animals were evaluated. (D) HG + HGFdf + ESA demonstrated a significantly reduced infarct size compared to PBS animals and smaller average infarcts compared to HG only animals. ANOVA with a Bonferroni correction for multiple comparisons, *p < 0.05.

Table 3
Large Animal Functional and Geometric Analysis.

	ED Mass (g)	ES Mass (g)	EDV (mL)	ESV (mL)	EF (%)
PBS	83.7 ± 14.4	86.3 ± 13.6	113.1 ± 23.3	77.9 ± 18.5	31.5 ± 3.0
	p = 0.240	p = 0.156	p = 0.850	p = 0.771	p = 0.664
HG Only	81.2 ± 7.3	83.3 ± 6.8	104.4 ± 10.0	69.9 ± 6.1	32.9 ± 2.1
	p = 0.399	p = 0.321	p = 0.895	p = 0.917	p = 0.986
HG + HGFdf + ESA	73.5 ± 10.6	75.0 ± 10.4	108.2 ± 13.6	72.8 ± 13.6	33.2 ± 4.7

ED, end diastolic; EDV, end-diastolic volume; EF, ejection fraction; ES, end systolic; ESV, end-systolic volume.

ventricular geometry in sheep that were treated with HG + HGFdf + ESA, though not statistically significant (Table 3). On average, HG + HGFdf + ESA demonstrated a reduced end diastolic mass (73.5 ± 10.6 g) and end systolic mass (75.0 ± 10.4 g) compared to both the HG only (81.2 ± 7.3 g and 83.3 ± 6.8, respectively) and PBS groups (83.7 ± 14.4 g and 86.3 ± 13.6, respectively). This may indicate a modest improvement in left ventricular remodeling. Other data indicated similar parameters between treatment groups, which elicits further investigation into dosing and necessitates larger sample sizes. Nonetheless, we determined that delivery of the HA-NP hydrogel containing engineered cytokines is feasible and translational.

5. Discussion

Myocardial ischemia and subsequent tissue death remain pervasive issues with few effective therapies available to prevent the onset of heart failure [1,2]. For the last few decades, cytokine and growth factor therapies have been rigorously investigated as adjunct treatments for myocardial infarction and heart failure [11,46–49]. However, none of these treatments have been translated to the clinic, and few are evaluated in large, clinically-relevant animal models, which may ultimately provide crucial information on how to effectively translate these therapeutics [50]. Additionally, a majority of these studies have utilized a single cytokine approach, which is limited in practice due to the complex mechanism of progressive adverse left ventricular remodeling [51–54]. In this study, we aimed to overcome many of the limitations of cytokine therapy for the treatment of myocardial ischemia and investigated the potential of a shear-thinning, catheter-deliverable hydrogel to deliver protein-engineered, optimized cytokines for sustained therapeutic effect. Furthermore, we validated this system in both a small and large animal model.

Growth factors and cytokines have been implemented in preclinical studies to induce regenerative mechanisms including angiogenesis [13,55–57], anti-apoptosis [15,16,29], and proliferation [58–60]. The goal of these therapies is to stimulate intrinsic repair pathways to limit the extent of damage caused by a myocardial infarction and subsequent infarct expansion [61]. While many of these therapies have demonstrated promise, protein therapeutics are limited by short half-lives *in vivo*, instability, rapid degradation, and diffusion away from the region of interest [28,37,40,45]. Furthermore, recombinant proteins are difficult to synthesize due to their large, complex structures and therefore can be expensive to manufacture, thereby decreasing clinical translatability [25,28,37]. To address these issues, our team developed protein-engineered variants of key cytokines, which confer increased stability,

enhanced activity, and simpler manufacturing processes [25,36,37].

Given that regeneration and repair are complex processes, we wanted to harness two different protein-engineered cytokines which target separate but synergistic pathways. The first protein-engineered polypeptide is a variant of SDF, called ESA, which is a miniaturized form that exhibits increased stability and activity compared to full-length SDF [8,36–38,45,62,63]. ESA is a potent chemokine which localizes EPCs to areas of ischemia, inducing a robust pro-angiogenic response, increasing myocyte survival, and preserving LV mechanical properties [37,38,45,64]. The second cytokine is an engineered form of HGF, called HGFdf, which has been demonstrated to have increased stability and increased expression yield compared to native HGF [28,40]. HGFdf stimulates pleiotropic behavior, exhibiting anti-apoptotic, anti-fibrotic, and pro-angiogenic effects [26,40]. We hypothesized that utilizing both cytokines would enhance the therapeutic response following myocardial infarction.

In addition to utilizing more stable and efficacious protein variants, we aimed to further enhance the translatability of this treatment strategy by utilizing a shear-thinning hydrogel. There has been a surge in the development of injectable hydrogels in the treatment of myocardial infarction and heart failure in the last decade [52,65]. The advantages of injectable hydrogels are multi-fold as these materials can (1) be applied as bulking agents to limit abnormal stress-strain distributions in the border zone region thereby limiting infarct expansion and preserving LV geometry, (2) localize therapeutics to the intended delivery region, (3) sustain delivery of therapeutics to prolong the beneficial response, (4) protect encapsulated therapeutics from rapid degradation and proteases, and (5) provide precise control over drug delivery [22,23,38,66–68]. However, very few hydrogels are amenable to catheter-based delivery, which is necessary for clinical translation. As a result, we recently developed a novel, highly shear-thinning, self-healing biocompatible HA-NP hydrogel that is capable of being injected through long, narrow clinically-relevant catheters and high gauge needles [24]. Additionally, this hydrogel is composed of FDA-approved products, is easily synthesized and scaled, and has multiple phases which lends to controlled drug delivery. This material is comprised of hydrophobically-modified HA crosslinked by biodegradable PEG-PLA nanoparticles, harnessing the biocompatible and intrinsic biological signaling properties of HA [69].

In this study, we encapsulated the two engineered cytokines into different phases of the HA-NP hydrogel to leverage spatio-temporal control over drug delivery. ESA was encapsulated into the NP phase of the hydrogel in order to normalize the temporal mismatch between expression of native SDF and its receptor CXCR4. On bone marrow and cardiac cells, CXCR4 expression peaks at 96 h following ischemia [38,70]; therefore, we aimed for a slower release of ESA. Further, in a previous small animal study, we concluded that prolonged release resulted in greater therapeutic benefit [38]. Conversely, because of the anti-apoptotic activity induced by HGFdf, we sought to implement a faster release by encapsulating into the aqueous phase to enable the maximum prevention of cardiomyocyte apoptosis. We determined that encapsulation of the cytokines within the different phases of the hydrogel preserved activity, produced distinct release profiles, and prolonged release. Impressively, the HA-NP hydrogel eluted ESA for over 30 days *in vitro* and eluted HGFdf for 28 days, successfully accomplishing our delivery timing for small animal translation.

Our next aim for this study was to evaluate the therapeutic efficacy of this approach in a small animal model of MI. Animals treated with HA-NP hydrogel encapsulating ESA and HGFdf (HG + HGFdf + ESA) exhibited a pronounced decrease in scar size, stimulated robust angiogenesis in the border zone regions, and preserved LV geometry and function. We also observed modest improvements in the HG only and HGFdf + ESA only groups, though were not as marked as the improvements in the combined treatment group. This is consistent with our previously published studies as well as literature supporting the observation that unloaded hydrogels can induce a therapeutic response by reinforcing the myocardium [38,40,71]. We also expect biochemical signaling behavior from the HA-NP hydrogel due to interaction of HA with the membrane protein CD44 on progenitor cells. Finally, we were able to observe all of the treatment components within the heart tissue for over 28 days, supporting our notion of sustained release.

Finally, due to the notable functional and biological benefits observed in the small animal study, we sought to complete a pilot study in a large animal preclinical model in order to evaluate the translatability of this therapeutic approach. Translating to large animals is a crucial step to optimize therapies prior to human clinical trials and provides crucial information on dosing, approach, and implementation. In a proof-of-concept study, we demonstrated that we were able to successfully deliver the HG + HGFdf + ESA treatment into the sheep tissue via a catheter-based approach, which resulted in a decrease in scar size eight weeks following myocardial infarction. While we did not observe a significant change in functional parameters, this pilot study will guide methodological changes and provided valuable insights into future studies. For instance, observing a significant decrease in scar size indicates that a therapeutic response is possible, but the therapeutic effect may need to be prolonged in order to induce a corresponding functional benefit. Considering our endpoint for this study was twice as long as the small animal study, we may need to alter the release profile of the therapeutics to achieve a longer release. This can be done by altering the strength (G') of the hydrogel. In our previous study, we demonstrated a 13-fold range in hydrogel strengths that can be accomplished with the HA-NP hydrogel composition [24] which provides a wide variety of release profiles. Additionally, this pilot study also prompts a deeper investigation of appropriate dosing for the large animals and longer timepoints. It is possible that a longer study needs to be performed in small animals to understand the appropriate dose. A limitation of this study is that we evaluated these therapeutics in an acute model of myocardial infarction, which does not accurately recapitulate the clinical scenario. Nonetheless, this study fulfills our scientific query of how the HA-NP hydrogel encapsulating protein-engineered cytokines affects ischemic myocardium and demonstrates how sustained, minimally-invasive delivery can be accomplished in the heart. In future studies, we will further optimize dosing, translate this to a fully endovascular approach, and evaluate in more chronic models to create a viable adjunct treatment for myocardial infarction and heart failure.

While we have observed numerous beneficial effects of this hydrogel delivery system, there are potential drawbacks that will need to be assessed. For example, hemocompatibility is an important criterion for any hydrogel being delivered via an endovascular approach. In a previous study, we evaluated the hemocompatibility using very small volumes of the hydrogel injected in the lumen of the left ventricle [24]. Even though no adverse effects were observed, we aim to repeat this experiment in greater volumes and in larger animal models. We will then be able to evaluate the impact of potential leakage of the hydrogel into the bloodstream. A second potential problem may arise due to the chemical composition of the hydrogel. We chose to utilize 1 MDa HA for the backbone of the hydrogel due to the anti-inflammatory effects of the high molecular weight of this polymer. However, lower molecular weight HA has reported to induce pro-inflammatory signals, which could occur if proteases degrade the hydrogel [72]. In this particular study, we did not observe any significant inflammation, but will need to evaluate this element in chronic models.

In summary, we have developed a novel, clinically-translatable hydrogel system which is capable of releasing individual cytokines with distinct release profiles. This combined therapeutic approach allows spatio-temporal delivery to target separate regenerative pathways which ultimately result in decreased scar formation, enhanced angiogenesis, and improved left ventricular function following ischemia.

CRediT authorship contribution statement

Amanda N. Steele: Conceptualization, Data curation, Investigation, Formal analysis, Validation, Visualization, Writing - original draft. **Michael J. Paulsen:** Conceptualization, Data curation, Investigation, Formal analysis, Validation, Visualization. **Hanjay Wang:** Conceptualization, Data curation, Investigation, Formal analysis, Validation, Visualization, Writing - original draft. **Lyndsay M. Stapleton:** Conceptualization, Data curation, Investigation, Formal analysis, Writing - original draft. **Haley J. Lucian:** Data curation, Investigation, Formal analysis, Validation, Visualization. **Anahita Eskandari:** Data curation, Investigation, Formal analysis, Validation, Visualization. **Camille E. Hironaka:** Data curation, Investigation, Formal analysis. **Justin M. Farry:** Data curation, Investigation, Formal analysis, Validation, Visualization. **Samuel W. Baker:** Data curation, Investigation, Formal analysis. **Akshara D. Thakore:** Data curation, Investigation, Formal analysis. **Kevin J. Jaatinen:** Data curation, Investigation, Formal analysis. **Yuko Tada:** Data curation, Investigation, Formal analysis, Validation, Visualization. **Michael J. Hollander:** Data curation, Investigation, Formal analysis. **Kiah M. Williams:** Data curation, Investigation, Formal analysis. **Alexis J. Seymour:** Data curation, Investigation, Formal analysis. **Kailey P. Totherow:** Data curation, Investigation, Formal analysis. **Anthony C. Yu:** Data curation, Investigation, Formal analysis. **Jennifer R. Cochran:** Conceptualization, Funding acquisition. **Eric A. Appel:** Conceptualization. **Y. Joseph Woo:** Conceptualization, Writing - original draft, Funding acquisition.

Declaration of Competing Interest

The authors declare that they have no known competing financial interests or personal relationships that could have appeared to influence the work reported in this paper.

Acknowledgements

This research was supported, in part, by the NIH R01CA151706 (Jennifer Cochran), Stanford ChEM-H Chemistry/Biology Interface Predoctoral Training Program (Michael Hollander), and National Cancer Institute NIH Award Number F31CA243267 (Michael Hollander).

Appendix A. Supplementary material

Supplementary data to this article can be found online at https://doi.org/10.1016/j.cyto.2019.154974.

References

[1] E.J. Benjamin, S.S. Virani, C.W. Callaway, A.M. Chamberlain, A.R. Chang, S. Cheng, et al., Heart disease and stroke statistics-2018 update: a report from the American Heart Association, Circulation 137 (2018) e67–e492, https://doi.org/10.1161/CIR.0000000000000558.

[2] E.J. Benjamin, P. Muntner, A. Alonso, M.S. Bittencourt, C.W. Callaway, A.P. Carson, et al., Heart disease and stroke statistics-2019 update: a report from the American Heart Association, Circulation 139 (2019) e56–e528, https://doi.org/10.1161/CIR.0000000000000659.

[3] L. Deveza, J. Choi, F. Yang, Therapeutic angiogenesis for treating cardiovascular diseases, Theranostics 2 (2012) 801–814, https://doi.org/10.7150/thno.4419.

[4] C. Steenbergen, N.G. Frangogiannis, Ischemic heart disease, Muscle, Elsevier, 2012, pp. 495–521 https://doi.org/10.1016/B978-0-12-381510-1.00036-3.

[5] G. Heusch, B.J. Gersh, The pathophysiology of acute myocardial infarction and strategies of protection beyond reperfusion: a continual challenge, Eur. Heart J. 38 (2017) 774–784, https://doi.org/10.1093/eurheartj/ehw224.

[6] M. Ejiri, M. Fujita, O. Sakai, K. Miwa, H. Asanoi, S. Sasayama, Development of collateral circulation after acute myocardial infarction: its role in preserving left ventricular function, J. Cardiol. 20 (1990) 31–37.

[7] J.T. Ortiz-Pérez, D.C. Lee, S.N. Meyers, C.J. Davidson, R.O. Bonow, E. Wu, Determinants of myocardial salvage during acute myocardial infarction: evaluation with a combined angiographic and CMR myocardial salvage index, JACC Cardiovasc. Imag. 3 (2010) 491–500, https://doi.org/10.1016/j.jcmg.2010.02.004.

[8] W. Hiesinger, A.B. Goldstone, Y.J. Woo, Re-engineered stromal cell-derived factor-1α and the future of translatable angiogenic polypeptide design, Trends Cardiovasc. Med. 22 (2012) 139–144, https://doi.org/10.1016/j.tcm.2012.07.010.

[9] L. Bolognese, N. Carrabba, G. Parodi, G.M. Santoro, P. Buonamici, G. Cerisano, et al., Impact of microvascular dysfunction on left ventricular remodeling and long-term clinical outcome after primary coronary angioplasty for acute myocardial infarction, Circulation 109 (2004) 1121–1126, https://doi.org/10.1161/01.CIR.0000118496.44135.A7.

[10] P. Garot, O. Pascal, M. Simon, J.L. Monin, E. Teiger, J. Garot, et al., Impact of microvascular integrity and local viability on left ventricular remodelling after reperfused acute myocardial infarction, Heart 89 (2003) 393–397, https://doi.org/10.1136/heart.89.4.393.

[11] P. Atluri, Y.J. Woo, Pro-angiogenic cytokines as cardiovascular therapeutics: assessing the potential, BioDrugs 22 (2008) 209–222, https://doi.org/10.2165/00063030-200822040-00001.

[12] X. Hao, E.A. Silva, A. Månsson-Broberg, K.-H. Grinnemo, A.J. Siddiqui, G. Dellgren, et al., Angiogenic effects of sequential release of VEGF-A165 and PDGF-BB with alginate hydrogels after myocardial infarction, Cardiovasc. Res. 75 (2007) 178–185, https://doi.org/10.1016/j.cardiores.2007.03.028.

[13] C.R.W. Kuhlmann, C.A. Schaefer, L. Reinhold, H. Tillmanns, A. Erdogan, Signalling mechanisms of SDF-induced endothelial cell proliferation and migration, Biochem. Biophys. Res. Commun. 335 (2005) 1107–1114, https://doi.org/10.1016/j.bbrc.2005.08.006.

[14] M.A. Retuerto, P. Schalch, G. Patejunas, J. Carbray, N. Liu, K. Esser, et al., Angiogenic pretreatment improves the efficacy of cellular cardiomyoplasty performed with fetal cardiomyocyte implantation, J. Thorac. Cardiovasc. Surg. 127 (2004) 1041–1049, https://doi.org/10.1016/j.jtcvs.2003.09.049 discussion 1049.

[15] H. Jin, J.M. Wyss, R. Yang, R. Schwall, The therapeutic potential of hepatocyte growth factor for myocardial infarction and heart failure, Curr. Pharm. Des. 10 (2004) 2525–2533.

[16] V. Jayasankar, Y.J. Woo, T.J. Pirolli, L.T. Bish, M.F. Berry, J. Burdick, et al., Induction of angiogenesis and inhibition of apoptosis by hepatocyte growth factor effectively treats postischemic heart failure, J. Card. Surg. 20 (2005) 93–101, https://doi.org/10.1111/j.0886-0440.2005.200373.x.

[17] P. Carmeliet, Angiogenesis in health and disease, Nat. Med. 9 (2003) 653–660, https://doi.org/10.1038/nm0603-653.

[18] N. Ashammakhi, S. Ahadian, M.A. Darabi, M. El Tahchi, J. Lee, K. Suthiwanich, et al., Minimally invasive and regenerative therapeutics, Adv. Mater. Weinheim. 31 (2019) e1804041, https://doi.org/10.1002/adma.201804041.

[19] M.K. Nguyen, D.S. Lee, Injectable biodegradable hydrogels, Macromol. Biosci. 10 (2010) 563–579, https://doi.org/10.1002/mabi.200900402.

[20] C. Loebel, C.B. Rodell, M.H. Chen, J.A. Burdick, Shear-thinning and self-healing hydrogels as injectable therapeutics and for 3D-printing, Nat. Protoc. 12 (2017) 1521–1541, https://doi.org/10.1038/nprot.2017.053.

[21] J.L. Ungerleider, K.L. Christman, Concise review: injectable biomaterials for the treatment of myocardial infarction and peripheral artery disease: translational challenges and progress, Stem Cells Transl. Med. 3 (2014) 1090–1099, https://doi.org/10.5966/sctm.2014-0049.

[22] M.J. Hernandez, K.L. Christman, Designing acellular injectable biomaterial therapeutics for treating myocardial infarction and peripheral artery disease, JACC Basic Transl. Sci. 2 (2017) 212–226, https://doi.org/10.1016/j.jacbts.2016.11.008.

[23] E. Ruvinov, J. Leor, S. Cohen, The promotion of myocardial repair by the sequential delivery of IGF-1 and HGF from an injectable alginate biomaterial in a model of acute myocardial infarction, Biomaterials 32 (2011) 565–578, https://doi.org/10.1016/j.biomaterials.2010.08.097.

[24] A.N. Steele, L.M. Stapleton, J.M. Farry, H.J. Lucian, M.J. Paulsen, A. Eskandari, et al., A biocompatible therapeutic catheter-deliverable hydrogel for in situ tissue engineering, Adv. Healthc. Mater. 8 (2019) e1801147, https://doi.org/10.1002/adhm.201801147.

[25] D.S. Jones, P.-C. Tsai, J.R. Cochran, Engineering hepatocyte growth factor fragments with high stability and activity as Met receptor agonists and antagonists, PNAS 108 (2011) 13035–13040, https://doi.org/10.1073/pnas.1102561108.

[26] V. Sala, T. Crepaldi, Novel therapy for myocardial infarction: can HGF/Met be beneficial? Cell. Mol. Life Sci. 68 (2011) 1703–1717, https://doi.org/10.1007/s00018-011-0633-6.

[27] S. Gallo, V. Sala, S. Gatti, T. Crepaldi, Hgf/met axis in heart function and cardioprotection, Biomedicines 2 (2014) 247–262, https://doi.org/10.3390/biomedicines2040247.

[28] C.J. Liu, D.S. Jones, P.-C. Tsai, A. Venkataramana, J.R. Cochran, An engineered dimeric fragment of hepatocyte growth factor is a potent c-MET agonist, FEBS Lett. 588 (2014) 4831–4837, https://doi.org/10.1016/j.febslet.2014.11.018.

[29] N. Zhou, Y. Wang, W. Cheng, Z. Yang, Hepatocyte growth factor (HGF) promotes cardiac stem cell differentiation after myocardial infarction by increasing mTOR activation in p27kip haploinsufficient mice, Genes Genom. 37 (2015) 905–912, https://doi.org/10.1007/s13258-015-0320-3.

[30] H. Meng, Y. Du, B. Chen, M.B. Toorabally, Z.M. Wang, N. Zhou, et al., Safety and efficacy of intracoronary Ad-HGF administration for treating severe coronary disease: results from long-term follow-up of a Phase I clinical trial, J. Clin. Trials 07 (2017), https://doi.org/10.4172/2167-0870.1000322.

[31] B.-R. Son, D. Zhao, L.A. Marquez-Curtis, N. Shirvaikar, M.Z. Ratajczak, A. Janowska-Wieczorek, SDF-1-CXCR4 and HGF-c-met axes regulate mobilization/recruitment to injured tissue of human mesenchymal stem cells, Blood 104 (11) (2004) 2331.

[32] A.B. Goldstone, C.E. Burnett, J.E. Cohen, M.J. Paulsen, A. Eskandari, B.E. Edwards, et al., SDF 1-alpha attenuates myocardial injury without altering the direct contribution of circulating cells, J. Cardiovasc. Transl. Res. 11 (2018) 274–284,

https://doi.org/10.1007/s12265-017-9772-y.
[33] T.K. Ho, X. Shiwen, D. Abraham, J. Tsui, D. Baker, Stromal-cell-derived factor-1 (SDF-1)/CXCL12 as potential target of therapeutic angiogenesis in critical leg ischaemia, Cardiol. Res. Pract. 2012 (2012) 143209, https://doi.org/10.1155/2012/143209.
[34] J. Yamaguchi, K.F. Kusano, O. Masuo, A. Kawamoto, M. Silver, S. Murasawa, et al., Stromal cell-derived factor-1 effects on ex vivo expanded endothelial progenitor cell recruitment for ischemic neovascularization, Circulation 107 (2003) 1322–1328, https://doi.org/10.1161/01.CIR.0000055313.77510.22.
[35] G. Zhang, Y. Nakamura, X. Wang, Q. Hu, L.J. Suggs, J. Zhang, Controlled release of stromal cell-derived factor-1 alpha in situ increases c-kit+ cell homing to the infarcted heart, Tissue Eng. 13 (2007) 2063–2071, https://doi.org/10.1089/ten.2006.0013.
[36] W. Hiesinger, J.R. Frederick, P. Atluri, R.C. McCormick, N. Marotta, J.R. Muenzer, et al., Spliced stromal cell-derived factor-1α analog stimulates endothelial progenitor cell migration and improves cardiac function in a dose-dependent manner after myocardial infarction, J. Thorac. Cardiovasc. Surg. 140 (2010) 1174–1180, https://doi.org/10.1016/j.jtcvs.2010.08.012.
[37] W. Hiesinger, J.M. Perez-Aguilar, P. Atluri, N.A. Marotta, J.R. Frederick, J.R. Fitzpatrick, et al., Computational protein design to reengineer stromal cell-derived factor-1α generates an effective and translatable angiogenic polypeptide analog, Circulation 124 (2011) S18–S26, https://doi.org/10.1161/CIRCULATIONAHA.110.009431.
[38] J.W. MacArthur, B.P. Purcell, Y. Shudo, J.E. Cohen, A. Fairman, A. Trubelja, et al., Sustained release of engineered stromal cell-derived factor 1-α from injectable hydrogels effectively recruits endothelial progenitor cells and preserves ventricular function after myocardial infarction, Circulation 128 (2013) S79–S86, https://doi.org/10.1161/CIRCULATIONAHA.112.000343.
[39] Y. Shudo, A.B. Goldstone, J.E. Cohen, J.B. Patel, M.S. Hopkins, A.N. Steele, et al., Layered smooth muscle cell-endothelial progenitor cell sheets derived from the bone marrow augment postinfarction ventricular function, J. Thorac. Cardiovasc. Surg. 154 (2017) 955–963, https://doi.org/10.1016/j.jtcvs.2017.04.081.
[40] A.N. Steele, L. Cai, V.N. Truong, B.B. Edwards, A.B. Goldstone, A. Eskandari, et al., A novel protein-engineered hepatocyte growth factor analog released via a shear-thinning injectable hydrogel enhances post-infarction ventricular function, Biotechnol. Bioeng. 114 (2017) 2379–2389, https://doi.org/10.1002/bit.26345.
[41] W.M. Gramlich, I.L. Kim, J.A. Burdick, Synthesis and orthogonal photopatterning of hyaluronic acid hydrogels with thiol-norbornene chemistry, Biomaterials 34 (2013) 9803–9811, https://doi.org/10.1016/j.biomaterials.2013.08.089.
[42] E.A. Appel, M.W. Tibbitt, M.J. Webber, B.A. Mattix, O. Veiseh, R. Langer, Self-assembled hydrogels utilizing polymer-nanoparticle interactions, Nat. Commun. 6 (2015) 6295, https://doi.org/10.1038/ncomms7295.
[43] J.A. Burdick, C. Chung, X. Jia, M.A. Randolph, R. Langer, Controlled degradation and mechanical behavior of photopolymerized hyaluronic acid networks, Biomacromolecules 6 (2005) 386–391, https://doi.org/10.1021/bm049508a.
[44] M.A. Serban, G. Yang, G.D. Prestwich, Synthesis, characterization and chondroprotective properties of a hyaluronan thioethyl ether derivative, Biomaterials 29 (2008) 1388–1399, https://doi.org/10.1016/j.biomaterials.2007.12.006.
[45] J.W. Macarthur, J.E. Cohen, J.R. McGarvey, Y. Shudo, J.B. Patel, A. Trubelja, et al., Preclinical evaluation of the engineered stem cell chemokine stromal cell-derived factor 1α analog in a translational ovine myocardial infarction model, Circ. Res. 114 (2014) 650–659, https://doi.org/10.1161/CIRCRESAHA.114.302884.
[46] N. Beohar, J. Rapp, S. Pandya, D.W. Losordo, Rebuilding the damaged heart: the potential of cytokines and growth factors in the treatment of ischemic heart disease, J. Am. Coll. Cardiol. 56 (2010) 1287–1297, https://doi.org/10.1016/j.jacc.2010.05.039.
[47] V.F.M. Segers, R.T. Lee, Protein therapeutics for cardiac regeneration after myocardial infarction, J. Cardiovasc. Transl. Res. 3 (2010) 469–477, https://doi.org/10.1007/s12265-010-9207-5.
[48] G. Srinivas, P. Anversa, W.H. Frishman, Cytokines and myocardial regeneration: a novel treatment option for acute myocardial infarction, Cardiol. Rev. 17 (2009) 1–9, https://doi.org/10.1097/CRD.0b013e31817bd7ab.
[49] J.de S. Rebouças, N.S. Santos-Magalhães, F.R. Formiga, Cardiac regeneration using growth factors: advances and challenges, Arq. Bras. Cardiol. 107 (2016) 271–275, https://doi.org/10.5935/abc.20160097.
[50] A.N. Steele, Y.J. Woo, From bench to clinic: translation of cardiovascular tissue engineering products to clinical applications, in: V. Serpooshan, S.M. Wu (Eds.), Cardiovascular Regenerative Medicine: Tissue Engineering and Clinical Applications, Springer International Publishing, Cham, 2019, pp. 125–140, , https://doi.org/10.1007/978-3-030-20047-3_7.
[51] W. Hiesinger, M.J. Brukman, R.C. McCormick, J.R. Fitzpatrick, J.R. Frederick, E.C. Yang, et al., Myocardial tissue elastic properties determined by atomic force microscopy after stromal cell-derived factor 1α angiogenic therapy for acute myocardial infarction in a murine model, J. Thorac. Cardiovasc. Surg. 143 (2012) 962–966, https://doi.org/10.1016/j.jtcvs.2011.12.028.
[52] A.A. Rane, K.L. Christman, Biomaterials for the treatment of myocardial infarction: a 5-year update, J. Am. Coll. Cardiol. 58 (2011) 2615–2629, https://doi.org/10.1016/j.jacc.2011.11.001.
[53] K.Y. DeLeon-Pennell, C.A. Meschiari, M. Jung, M.L. Lindsey, Matrix metalloproteinases in myocardial infarction and heart failure, Prog. Mol. Biol. Transl. Sci. 147 (2017) 75–100, https://doi.org/10.1016/bs.pmbts.2017.02.001.
[54] J.A. Ambrose, M. Singh, Pathophysiology of coronary artery disease leading to acute coronary syndromes, F1000Prime Rep. 7 (08) (2015), https://doi.org/10.12703/P7-08.
[55] Z. Taimeh, J. Loughran, E.J. Birks, R. Bolli, Vascular endothelial growth factor in heart failure, Nat. Rev. Cardiol. 10 (2013) 519–530, https://doi.org/10.1038/nrcardio.2013.94.
[56] S. Cavallero, H. Shen, C. Yi, C.-L. Lien, S.R. Kumar, H.M. Sucov, CXCL12 signaling is essential for maturation of the ventricular coronary endothelial plexus and establishment of functional coronary circulation, Dev. Cell 33 (2015) 469–477, https://doi.org/10.1016/j.devcel.2015.03.018.
[57] K. Tachibana, S. Hirota, H. Iizasa, H. Yoshida, K. Kawabata, Y. Kataoka, et al., The chemokine receptor CXCR4 is essential for vascularization of the gastrointestinal tract, Nature 393 (1998) 591–594, https://doi.org/10.1038/31261.
[58] X. Liu, X. Gu, Z. Li, X. Li, H. Li, J. Chang, et al., Neuregulin-1/erbB-activation improves cardiac function and survival in models of ischemic, dilated, and viral cardiomyopathy, J. Am. Coll. Cardiol. 48 (2006) 1438–1447, https://doi.org/10.1016/j.jacc.2006.05.057.
[59] K. Bersell, S. Arab, B. Haring, B. Kühn, Neuregulin1/ErbB4 signaling induces cardiomyocyte proliferation and repair of heart injury, Cell 138 (2009) 257–270, https://doi.org/10.1016/j.cell.2009.04.060.
[60] J.E. Cohen, B.P. Purcell, J.W. MacArthur, A. Mu, Y. Shudo, J.B. Patel, et al., A bioengineered hydrogel system enables targeted and sustained intramyocardial delivery of neuregulin, activating the cardiomyocyte cell cycle and enhancing ventricular function in a murine model of ischemic cardiomyopathy, Circ. Heart Fail. 7 (2014) 619–626, https://doi.org/10.1161/CIRCHEARTFAILURE.113.001273.
[61] K. Kobayashi, K. Maeda, M. Takefuji, R. Kikuchi, Y. Morishita, M. Hirashima, et al., Dynamics of angiogenesis in ischemic areas of the infarcted heart, Sci. Rep. 7 (2017) 7156, https://doi.org/10.1038/s41598-017-07524-x.
[62] J.W. MacArthur, A. Trubelja, Y. Shudo, P. Hsiao, A.S. Fairman, E. Yang, et al., Mathematically engineered stromal cell-derived factor-1α stem cell cytokine analog enhances mechanical properties of infarcted myocardium, J. Thorac. Cardiovasc. Surg. 145 (2013) 278–284, https://doi.org/10.1016/j.jtcvs.2012.09.080.
[63] B.B. Edwards, A.S. Fairman, J.E. Cohen, J.W. MacArthur, A.B. Goldstone, J.B. Woo, et al., Biochemically engineered stromal cell-derived factor 1-alpha analog increases perfusion in the ischemic hind limb, J. Vasc. Surg. 64 (2016) 1093–1099, https://doi.org/10.1016/j.jvs.2015.06.140.
[64] H. Wang, A. Wisneski, M.J. Paulsen, A. Imbrie-Moore, Z. Wang, Y. Xuan, et al., Bioengineered analog of stromal cell-derived factor 1α preserves the biaxial mechanical properties of native myocardium after infarction, J. Mech. Behav. Biomed. Mater. 96 (2019) 165–171, https://doi.org/10.1016/j.jmbbm.2019.04.014.
[65] E. Tous, J.L. Ifkovits, K.J. Koomalsingh, T. Shuto, T. Soeda, N. Kondo, et al., Influence of injectable hyaluronic acid hydrogel degradation behavior on infarction-induced ventricular remodeling, Biomacromolecules 12 (2011) 4127–4135, https://doi.org/10.1021/bm201198x.
[66] C.B. Rodell, M.E. Lee, H. Wang, S. Takebayashi, T. Takayama, T. Kawamura, et al., Injectable shear-thinning hydrogels for minimally invasive delivery to infarcted myocardium to limit left ventricular remodeling, Circ. Cardiovasc. Interv. 9 (2016), https://doi.org/10.1161/CIRCINTERVENTIONS.116.004058.
[67] J.L. Ifkovits, E. Tous, M. Minakawa, M. Morita, J.D. Robb, K.J. Koomalsingh, et al., Injectable hydrogel properties influence infarct expansion and extent of post-infarction left ventricular remodeling in an ovine model, PNAS 107 (2010) 11507–11512, https://doi.org/10.1073/pnas.1004097107.
[68] T.D. Johnson, K.L. Christman, Injectable hydrogel therapies and their delivery strategies for treating myocardial infarction, Exp. Opin. Drug Deliv. 10 (2013) 59–72, https://doi.org/10.1517/17425247.2013.739156.
[69] J.A. Burdick, G.D. Prestwich, Hyaluronic acid hydrogels for biomedical applications, Adv. Mater. Weinheim. 23 (2011) H41–H56, https://doi.org/10.1002/adma.201003963.
[70] M.S. Penn, Importance of the SDF-1:CXCR4 axis in myocardial repair, Circ. Res. 104 (2009) 1133–1135, https://doi.org/10.1161/CIRCRESAHA.109.198929.
[71] H. Wang, C.B. Rodell, X. Zhang, N.N. Dusaj, J.H. Gorman, J.J. Pilla, et al., Effects of hydrogel injection on borderzone contractility post-myocardial infarction, Biomech. Model. Mechanobiol. 17 (2018) 1533–1542, https://doi.org/10.1007/s10237-018-1039-2.
[72] J.E. Rayahin, J.S. Buhrman, Y. Zhang, T.J. Koh, R.A. Gemeinhart, High and low molecular weight hyaluronic acid differentially influence macrophage activation, ACS Biomater. Sci. Eng. 1 (2015) 481–493, https://doi.org/10.1021/acsbiomaterials.5b00181.